

# Extremely Large Lamb Shift in a Deep-strongly Coupled Circuit QED System with a Multimode Resonator

Ziqiao Ao,<sup>1,2,3</sup> Sahel Ashhab,<sup>3</sup> Fumiki Yoshihara,<sup>3,4</sup> Tomoko Fuse,<sup>3</sup> Kosuke Kakuyanagi,<sup>5</sup> Shiro Saito,<sup>5</sup> Takao Aoki,<sup>1</sup> and Kouichi Semba<sup>3</sup>

<sup>1</sup>*Department of Applied Physics, Waseda University,*

*Okubo 3-4-1, Shinjuku-ku, Tokyo 169-8555, Japan*

<sup>2</sup>*Department of Advanced Science and Engineering,*

*Waseda University, 3-4-1 Okubo, Shinjuku-ku, Tokyo 169-8555, Japan*

<sup>3</sup>*Advanced ICT Institute, National Institute of*

*Information and Communications Technology, 4-2-1,*

*Nukuikitamachi, Koganei, Tokyo 184-8795, Japan*

<sup>4</sup>*Department of Physics, Tokyo University of Science,*

*1-3 Kagurazaka, Shinjuku-ku, Tokyo 162-8601, Japan*

<sup>5</sup>*NTT Basic Research Laboratories,*

*NTT Corporation, 3-1 Morinosato-Wakamiya,*

*Atsugi, Kanagawa 243-0198, Japan*

## Abstract

We report experimental and theoretical results on the extremely large Lamb shift in a multimode circuit quantum electrodynamics (QED) system in the deep-strong coupling (DSC) regime, where the qubit-resonator coupling strength is comparable to or larger than the qubit and resonator frequencies. The system comprises a superconducting flux qubit (FQ) and a quarter-wavelength coplanar waveguide resonator ( $\lambda/4$  CPWR) that are coupled inductively through a shared edge that contains a Josephson junction to achieve the DSC regime. Spectroscopy is performed around the frequency of the fundamental mode of the CPWR, and the spectrum is fitted by the single-mode quantum Rabi Hamiltonian to obtain the system parameters. Since the qubit is also coupled to a large number of higher modes in the resonator, the single-mode fitting does not provide the bare qubit energy but a value that incorporates the renormalization from all the other modes. We derive theoretical formulas for the Lamb shift in the multimode resonator system. As shown in previous studies, there is a cut-off frequency  $\omega_{\text{cutoff}}$  for the coupling between the FQ and the modes in the CPWR, where the coupling grows as  $\sqrt{\omega_n}$  for  $\omega_n/\omega_{\text{cutoff}} \ll 1$  and decreases as  $1/\sqrt{\omega_n}$  for  $\omega_n/\omega_{\text{cutoff}} \gg 1$ . Here  $\omega_n$  is the frequency of the  $n$ th mode. The cut-off effect occurs because the qubit acts as an obstacle for the current in the resonator, which suppresses the current of the modes above  $\omega_{\text{cutoff}}$  at the location of the qubit and results in a reduced coupling strength. Using our observed spectrum and theoretical formulas, we estimate that the Lamb shift from the fundamental mode is 82.3% and the total Lamb shift from all the modes is 96.5%. This result illustrates that the coupling to the large number of modes in a CPWR yields an extremely large Lamb shift but does not suppress the qubit energy to zero, which would happen in the absence of a high-frequency cut-off.

## Introduction

The interaction between an atom and an electromagnetic (EM) field has been actively studied not only to understand novel quantum physics phenomena but also to develop quantum communication and information processing technologies [1–3]. One well-known and well-studied phenomenon caused by this interaction is the Lamb shift [4], where the energy of the atom is slightly renormalized by the coupling with the vacuum fluctuations, which have so-called "half-photon" energy [5, 6]. When the coupling strength is pushed into stronger regimes [7, 8] such as the ultra-strong coupling (USC) or deep-strong coupling (DSC) regimes, the Lamb shift is no longer a small correction but a dominant contribution that drastically changes the atomic energy [9, 10].

Among several systems that can reach the USC and DSC regimes [11–14], superconducting quantum circuits (SQC) [15–17] are well suited for investigating the Lamb shift, because the USC and DSC regimes can be achieved using a single (artificial) atom (or qubit) coupled to either a single-mode or a multimode superconducting resonator [9, 10, 18–23]. In particular, multimode systems are attractive for the study of novel phenomena such as many-body effects [24–27] and photon frequency conversion [28]. Understanding the Lamb shift in a multimode DSC system is an important step to establish better control over such a complex system.

In this work, to study the Lamb shift caused by the coupling between an artificial atom and a multimode resonator in the DSC regime, we investigated circuit QED systems where a FQ is coupled to a  $\lambda/4$  CPWR. The qubit and the resonator are coupled inductively through a shared-edge with a Josephson junction inserted to induce a large inductance and enhance the coupling strength in order to reach the DSC regime [9, 19, 29, 30]. We conducted spectroscopy experiment on our system around the fundamental mode frequency. By using the single-mode quantum Rabi model (QRM), we can fit the spectrum with the QRM Hamiltonian and obtain the system parameters. The fitting provides the qubit's bare frequency, the resonator frequency and the coupling strength. The obtained qubit frequency is a renormalized one rather than the truly bare one, the reason being the renormalization from all the other modes in the resonator that are not included explicitly in our single-mode QRM Hamiltonian. We have developed the theoretical model for our system. In spite of difference in the circuit design and qubit-resonator coupling mechanism, we obtain similar

results in our system as in previously studied multimode circuit QED systems [31, 32]. In particular, a cut-off effect arises naturally, such that the coupling strength between the qubit and the different modes is suppressed for high-frequency modes. This cut-off effect prevents the qubit frequency from being suppressed to zero, which would happen if the qubit were coupled to an infinite number of resonator modes with no cut-off in the coupling strength. We also derived a formula for the total amount of the Lamb shift induced by all the modes in a multimode resonator.

## Results

Figure 1 shows the schematics of our circuit QED system. The CPWR is coupled to a transmission line (TL) through the mutual inductance (M in Fig. 1 (b)). The spectroscopy microwave signal is applied through the TL, and the transmitted signal is measured. The FQ is placed at the short end of the  $\lambda/4$  CPWR to couple with all the modes and a Josephson junction, which works as a simple inductance  $L_C$ , is placed at the shared edge to enhance the coupling strength to achieve DSC [19]. Note that in this particular design, the coupling Josephson junction is split into parallel ones due to the difficulty to fabricate a large one, which results in a similar effect of a SQUID. Due to the area difference between the FQ loop and the SQUID loop, the frequency modulation by the coupling SQUID is distinguishable from the modulation by the qubit.

The transmission spectrum around the fundamental mode frequency is shown in Fig. 2. For the fitting of the spectrum, we used following single-mode quantum Rabi Hamiltonian

$$\mathcal{H}_1 = -\frac{1}{2}(\Delta'_0\sigma_X + \varepsilon\sigma_Z) + \omega_1 a_1^\dagger a_1 + g_1\sigma_Z(a_1 + a_1^\dagger). \quad (1)$$

Note that we take  $\hbar = 1$ . Here,  $\Delta'_0$  is the qubit energy renormalized by all the resonator modes except the fundamental mode.  $\varepsilon$  is the flux bias between the two qubit persistent current states,  $|R\rangle$  and  $|L\rangle$ .  $\omega_1$  is the mode energy of the fundamental mode in the CPWR, and  $g_1$  is the coupling energy between the qubit and the fundamental mode.  $\sigma_X$  and  $\sigma_Z$  are Pauli operators and  $a^\dagger$  and  $a$  are creation and annihilation operator, respectively. Since the modes are discrete and each mode renormalizes the qubit energy, the single-mode QRM Hamiltonian can provide good approximations for the circuit parameters around the fundamental mode frequency, except for the fact that  $\Delta'_0$  is not the bare qubit energy  $\Delta_0$ .

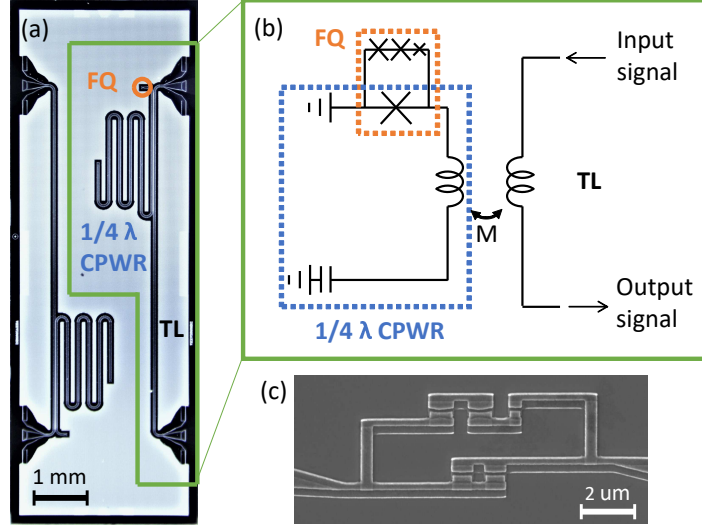


FIG. 1: (a) Microscope image of the chip. The chip contains two sets of independent circuit QED systems. Each of the system is inductively coupled to an independent TL. (b) Model of a single circuit QED system. The CPWR is inductively coupled to the TL through the mutual inductance  $M$ . Spectroscopy signal is input from one side of the TL and the output signal transmitted to the other side is measured. (c) SEM image of the qubit loop. There are three Josephson junctions in the upper part of the loop as the conventional ones for a FQ and two Josephson junctions in the lower part of the loop acting as the coupling junction.

By fitting the theory curves to the measured spectrum, we obtained the circuit parameters as  $\omega_1/2\pi = 2.57$  GHz,  $\Delta'_0/2\pi = 0.147$  GHz and  $g_1/2\pi = 2.39$  GHz. The qubit energy renormalized by all the modes corresponds to the transition frequency  $\omega_{01}$  at the optimal bias point ( $\epsilon = 0$ ). Here  $\omega_{ij}$  is the frequency of the transition  $|i\rangle \leftrightarrow |j\rangle$ . Although  $\omega_{01}$  at  $\epsilon = 0$  is smaller than the measurable range of our experimental set-up and hence cannot be measured directly, it can be calculated straightforwardly by taking the difference  $\omega_{03} - \omega_{13}$ , which yields  $\omega_{01}/2\pi = 26$  MHz.

To calculate the amount of the Lamb shift induced by multiple modes in the resonator, we derived a formula for the Lamb shift within the theoretical framework that describes the natural cut-off of the coupling for high-frequency modes. We start by considering the circuit QED system shown in Fig. 3 (a) which serves as a theoretical model for the experimental setup (Fig. 1) without the TL.

Approximating the coupling Josephson junction as a linear inductance  $L_C$  and the two

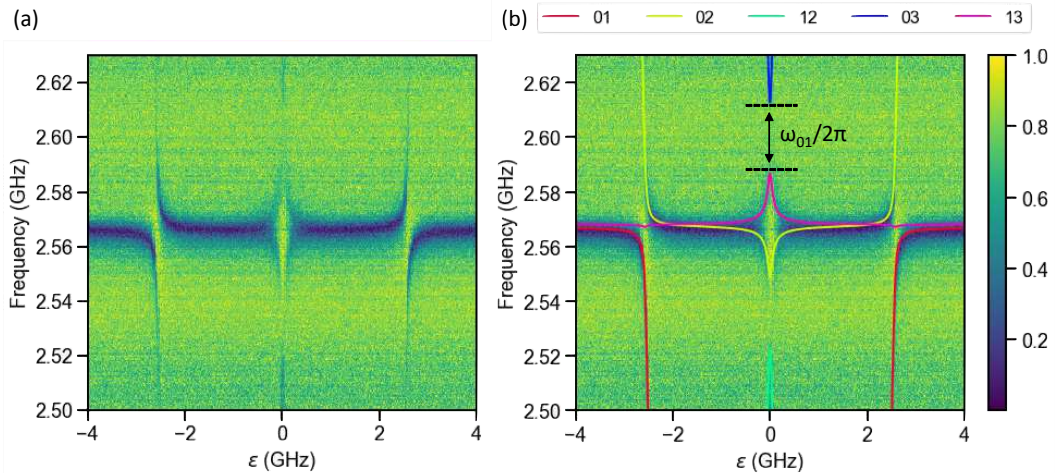


FIG. 2: (a) Measured spectrum. x-axis is the flux bias in frequency and y-axis is the probe frequency. The color bar shows the normalized amplitude of measured output signal. (b) Same spectrum along with theory curves calculated using Eq. (1) and optimized fitting parameters:  $\omega_1/2\pi = 2.57$  GHz,  $\Delta'_0/2\pi = 0.147$  GHz and  $g_1/2\pi = 2.39$  GHz. The labels of the theory curves indicates the transitions between pairs of energy eigenstates. In particular, the pair 01 means the transition from the ground state  $|0\rangle$  to the first excited state  $|1\rangle$  of the system. The frequency  $\omega_{01}$  is the renormalized qubit frequency.

big FQ junctions together as a linear inductance  $L_2$  (respectively the red one and two blue ones in Fig. 3 (a)) for simplicity, the Lagrangian of this circuit can be expressed as

$$\mathcal{L} = \frac{1}{2}C_q\dot{\Phi}^2 + U_q(\Phi, \Phi_{\text{ext}}) + \sum_{j=0}^N \left( \frac{1}{2}c\dot{\phi}_j^2 - \frac{1}{2l}(\phi_j - \phi_{j+1})^2 \right) - \frac{1}{2L_c}\dot{\phi}_0^2 - \frac{1}{2L_2}(\Phi - \phi_0)^2. \quad (2)$$

Here,  $\Phi$  is the flux at the node at the right side of the small junction in the qubit loop and  $\phi_j$  is the flux at the node  $j$  ( $j = 0, 1, 2, \dots, N$ ) of the CPWR.  $C_q$  is the capacitance of the small blue junction in Fig. 3 (a) and  $U_q(\Phi, \Phi_{\text{ext}}) = \alpha E_J \cos \{2\pi(\Phi - \Phi_{\text{ext}})/\Phi_0\}$  is the effective Josephson potential for the small Josephson junction.  $\alpha$  is the area ratio of the small junction,  $E_J = I_c\Phi_0/(2\pi)$  is the Josephson energy of the large junctions,  $I_c$  is the critical current of the Josephson junction and  $\Phi_0 = h/(2e)$  is the superconducting flux quantum.  $c$  and  $l$  are, respectively, the capacitance and the inductance per unit length of the resonator. Using the Legendre transformation,  $Q = \partial\mathcal{L}/\partial\dot{\Phi} = C_q\dot{\Phi}$  and  $q_j = \partial\mathcal{L}/\partial\dot{\phi}_j = c\dot{\phi}_j$ , the Hamiltonian of the circuit can be obtained as

$$\mathcal{H} = \frac{1}{2C_q}Q^2 - U_q(\Phi, \Phi_{\text{ext}}) + \sum_{j=0}^N \left( \frac{1}{2c}q_j^2 + \frac{1}{2l}(\phi_j - \phi_{j+1})^2 \right) + \frac{1}{2L_c}\dot{\phi}_0^2 + \frac{1}{2L_2}(\Phi - \phi_0)^2. \quad (3)$$

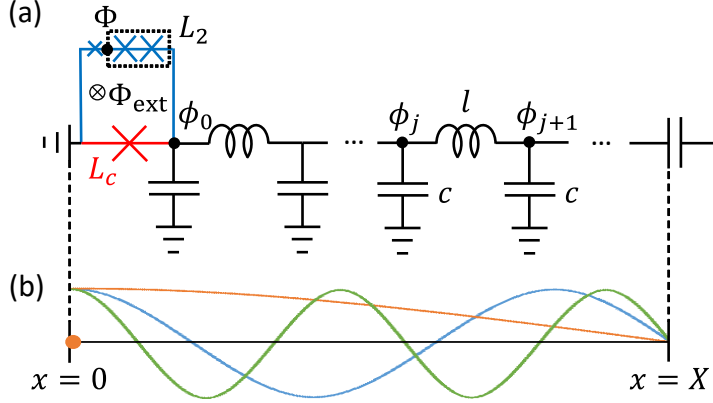


FIG. 3: (a) Theoretical model for the circuit QED system. The loop formed by the blue and red segments are the FQ loop, while the black and red parts form the CPWR. The red part is the edge that is shared by the FQ and the CPWR with a Josephson junction inserted to achieve the DSC regime. (b) Lowest three modes in the CPWR. The color of the lines indicate the fundamental (orange), the second (blue) and the third (green) modes. The orange dot indicates the location of the qubit where the qubit can couple to all modes in the CPWR. Note that the scales of the two figures are different.

By ignoring the qubit term, represented by the variables  $\Phi$  and  $Q$ , the equations of motions yield

$$\omega_{\text{cutoff}} = \frac{Z_0}{L_{C2}}. \quad (4)$$

with consideration of the boundary conditions at  $x = 0$  and  $x = X$  (more details in Method section). Here,  $Z_0 = \sqrt{l/c}$  is the characteristic impedance of the CPWR and  $L_{C2} = L_c L_2 / (L_c + L_2)$ . Since  $L_c \ll L_2$ ,  $L_{C2}$  can be approximated as  $L_c$ . This result is consistent with previous results in the literature [31, 32], although a different circuit design and capacitive coupling between a transmon qubit and a CPWR were considered in those studies.

From the mode frequencies and wave functions, we calculated the zero-point fluctuation of the current  $I_n^{\text{Zpf}}$  for the  $n$ th mode to obtain the coupling strength between the qubit and the  $n$ th mode as  $g_n = L_c I_q I_n^{\text{Zpf}}$ , where  $I_q$  is the qubit persistent current [9, 30]. Then  $I_n^{\text{Zpf}}$  can be described as

$$I_n^{\text{Zpf}} = \sqrt{\frac{1}{L}} \sqrt{\frac{\omega_n}{1 + \left(\frac{\omega_n}{\omega_{\text{cutoff}}}\right)^2}}. \quad (5)$$

Here  $L = Xl$  is the total inductance of the CPWR and  $\omega_n$  is the bare frequency of the  $n$ th

mode. More information is given in the Methods section. This equation shows that for the low-frequency modes ( $\omega_n \ll \omega_{\text{cutoff}}$ ),  $g_n \propto \sqrt{\omega_n}$ , and for the high-frequency case ( $\omega_n \gg \omega_{\text{cutoff}}$ ),  $g_n \propto 1/\sqrt{\omega_n}$ . Figure 4 (a) shows how  $g_n$  grows as the mode frequency increases with different coupling inductance  $L_c$ . Here we used the parameters for the calculation which we took from the circuit design: the total inductance of the resonator  $L = 1.93$  nH,  $L_2 = 823$  pH,  $\alpha = 0.46$ , and  $E_J = 397$  GHz.

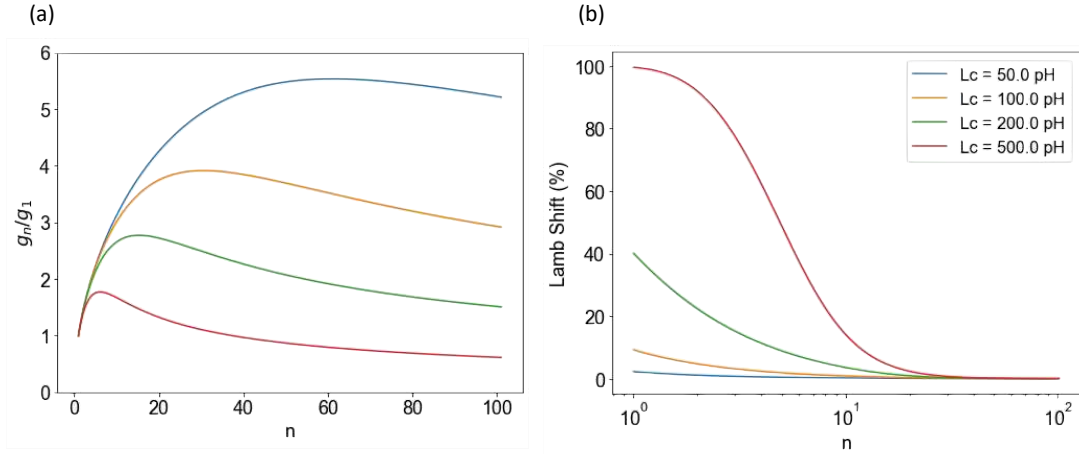


FIG. 4: (a) Normalized coupling strength  $g_n/g_1$  with each mode. The mode which gives the biggest  $g_n$  in each line indicates it is the mode where cut-off effect occurs. The plots shows that bigger  $L_c$  yields smaller  $\omega_{\text{cutoff}}$  as described in Eq. (4). The color of the lines follows the legend in (b). (b) Lamb shift induced by each mode. The lines show that how much Lamb shift each mode induces to  $\Delta_0$ . As the mode number grows, less amount of Lamb shift will be induced due to smaller  $g_n$  caused by the cut-off effect. Note that the x-axis is plotted in logarithmic scale.  $L = 1.93$  nH,  $L_2 = 823$  pH,  $\alpha = 0.46$ , and  $E_J = 397$  GHz are used for the plots.

Now we derive the formula for the Lamb shift caused by the multiple modes in the CPWR using the formula for  $g_n$ . For the single-mode case, a large Lamb shift has been reported using a FQ-lumped element resonator (LCR) system in the DSC regime with inductive coupling [9, 29]. The renormalized qubit energy  $\Delta$  can be expressed as a function of the bare qubit energy  $\Delta_0$ , the resonant frequency  $\omega$  of the resonator mode and the coupling strength  $g$ :

$$\Delta = \Delta_0 \exp(-2g^2/\omega^2) \quad (6)$$

which is valid when  $\Delta_0 \ll \omega$  [33]. Here the relative Lamb shift is calculated as  $(\Delta_0 - \Delta)/\Delta_0$ .

When a CPWR is used and the FQ is assumed to couple to multiple modes,  $\Delta_0$  will be renormalized by all modes in the CPWR and  $\Delta$  can be expressed by the product of all the exponential terms induced by the modes as

$$\Delta = \Delta_0 \prod_n \exp(-2g_n^2/\omega_n^2) = \Delta_0 \exp\left(-2 \sum_n g_n^2/\omega_n^2\right). \quad (7)$$

Here,  $g_n$  is the coupling strength between the FQ and the  $n$ th mode. Using Eq. (5) with the formula for  $g_n$  and taking into consideration that the mode frequencies in a  $\lambda/4$  CPWR are odd multiples of the fundamental-mode frequency, Eq. (7) can be transformed into

$$\Delta = \Delta_0 \exp\left\{-2 \left(\frac{g_1}{\omega_1}\right)^2 \sum_{n=1,3,\dots} \frac{1}{n \left(1 + \frac{n^2}{n_{\text{cutoff}}^2}\right)}\right\}. \quad (8)$$

Here  $n_{\text{cutoff}} = \omega_{\text{cutoff}}/\omega_1$ . Comparing with Eq. (6), which describe the single-mode case, Eq. (8) has an additional sum term in the exponential, which enhances the total Lamb shift compared to the single-mode value. Figure 4 (b) shows the Lamb shift that each mode induces in  $\Delta_0$ . If we take  $\Delta_n$  as the renormalized qubit energy by the  $n$ th mode only, the amount of the Lamb shift caused by the  $n$ th mode can be described as  $(\Delta_0 - \Delta_n)/\Delta_0$ . Using the software package Mathematica, we find that the sum in Eq. (8) approaches  $0.25(2\gamma + \log 4) + 0.5\log n_{\text{cutoff}}$ , where  $\gamma$  is Euler's constant, in the limit  $n_{\text{cutoff}} \rightarrow \infty$ . Put differently, the sum can be very well approximated by the simple formula  $0.635 + 0.5\log n_{\text{cutoff}}$ , provided that  $n_{\text{cutoff}} \gg 1$ . The replacement of the sum by this simple formula illustrates the important point that we do not need to characterize the coupling between the qubit and every resonator mode individually. The system parameters that we obtained using the single-mode model including only the fundamental mode allows us to estimate the total Lamb shift contributed by all the modes. Using the value of the impedance  $Z_0 = 50 \Omega$  of the resonator and the coupling inductance  $L_C = 231 \text{ pH}$ , we estimate that  $\omega_{\text{cutoff}}/2\pi \sim 34.4 \text{ GHz}$ , or alternatively  $n_{\text{cutoff}} = 13.2$ . Note that  $L_C$  is calculated from the difference between the designed bare fundamental mode frequency and the measured fundamental mode frequency at the zero flux point. In this case, the sum in Eq. (8) yields 1.93. Using the system parameters obtained from the fitting, we find that the total Lamb shift in our multimode system is 96.5%. Using this result and the measured  $\Delta/2\pi = 26 \text{ MHz}$ , the bare qubit energy can be calculated as  $\Delta_0/2\pi \sim 732 \text{ MHz}$ .

## Discussion

We obtained experimental and theoretical results pertaining to the extremely large Lamb shift that occurs in a DSC multimode circuit QED system containing a superconducting FQ and a CPWR. We used the single-mode quantum Rabi Hamiltonian to fit the measured spectrum at the fundamental mode to obtain the circuit parameters. The measured spectrum shows that our system is in the DSC regime. The single-mode QRM model was used to obtain the system parameters. The fitting gave the fully renormalized qubit energy as  $\Delta/2\pi = 26$  MHz. We considered the cut-off effect for the coupling strength  $g_n$  and showed theoretically that  $g_n$  decreases at  $\omega_n \gg \omega_{\text{cutoff}}$  in our system, similarly to the cut-off effect obtained with different circuit designs. We derived the formula for the renormalized qubit energy  $\Delta$  which yields the Lamb shift. Our theoretical results demonstrate how  $\Delta$  survives the renormalization by the Lamb shift and remains finite even in the case of strong coupling to an infinite number of modes in a CPWR. The total Lamb shift in our system was calculated to be 96.5%, which is larger than the values measured previously using single-mode resonators.

## Methods

### Derivation of the cutoff frequency

To find the modes in the CPWR, a standard approach is to ignore qubit terms (i.e.  $\Phi$ ) in the first-order and second-order of equations of motion, which gives

$$\frac{\partial^2 \phi}{\partial t^2} = \frac{1}{cl} \frac{\partial^2 \phi}{\partial x^2} \quad (9)$$

$$\left( \frac{1}{X^2 cl} \frac{\partial \phi}{\partial x} - \frac{\phi}{X c L_C} - \frac{\phi}{X c L_2} \right) \Big|_{x=0} = 0 \quad (10)$$

$$\left. \frac{\partial \phi}{\partial x} \right|_{x=X} = 0. \quad (11)$$

$x$  indicates the location in the CPWR with the two boundary,  $x = 0$  and  $x = X$ . By substituting a solution  $\phi(x, t) = e^{i\omega t} u(x)$  with a temporal frequency  $\omega$  and time  $t$  in these equations, we obtain

$$-\omega^2 u(x) = \frac{1}{cl} \frac{\partial^2 u}{\partial x^2} \quad (12)$$

$$\left( \frac{1}{cl} \frac{\partial u}{\partial x} - \frac{u}{c L_{C2}} \right) \Big|_{x=0} = 0 \quad (13)$$

$$\left. \frac{\partial u}{\partial x} \right|_{x=X} = 0 \quad (14)$$

with  $L_{C2} = L_C L_2 / (L_C + L_2)$ . The solution of Eq. (12) can be written as  $u(x) = u_C \cos(kx) + u_S \sin(kx)$ , where  $k = \sqrt{\omega^2 cl}$ . The boundary conditions Eq. (13) and Eq. (14) now give us  $k \tan(kX) = l/L_{C2}$ , in other form,

$$\omega \tan(kX) = \omega_{\text{cutoff}} \quad (15)$$

where

$$\omega_{\text{cutoff}} = \frac{Z_0}{L_{C2}}. \quad (16)$$

Here,  $Z_0 = \sqrt{l/c}$  is the characteristic impedance of the CPWR.

### Derivation of the zero-point fluctuation of the current

For the low-frequency modes which frequency is less than  $\omega_{\text{cutoff}}$ , the solutions of Eq. (15) must have  $\tan(kX) \gg 1$ , which allow us to make the approximation that  $kX$  is close to  $n\pi - \pi/2$ , where  $n$  is the mode number starting at  $n = 1$  for the fundamental mode. After defining  $k\tilde{X} = n\pi - \pi/2 - kX$ , the solutions can be written as

$$k\tilde{X} = n\pi - \frac{\pi}{2} - X\sqrt{cl}\omega_{\text{cutoff}} \cot\left(n\pi - \frac{\pi}{2} - k\tilde{X}\right).$$

Making the approximation that  $\cot(n\pi - \pi/2 - \delta) \approx \delta$  gives the first-order approximation in  $\omega/\omega_{\text{cutoff}}$  as

$$k\tilde{X} \approx \frac{n\pi - \frac{\pi}{2}}{1 + X\sqrt{cl}\omega_{\text{cutoff}}} \quad (17)$$

and therefore

$$kX \approx n\pi - \frac{\pi}{2} - \frac{\left(n\pi - \frac{\pi}{2}\right)}{X\sqrt{cl}\omega_{\text{cutoff}}} = \left(n\pi - \frac{\pi}{2}\right) \times \left(1 - \frac{L_{C2}}{Xl}\right) \quad (18)$$

which gives us the frequency of the fundamental mode  $\omega_1 = \pi/2X\sqrt{cl}$  as expected for a quarter-wavelength CPWR.

The energy  $E_n$  of each mode can be found in the Hamiltonian proportional to  $u_C^2$  as

$$E_n = \frac{Xk^2 u_C^2}{2l}. \quad (19)$$

In the ground state of each mode, the energy of each mode should also be  $E_n = \hbar\omega_n/2$ , which therefore gives the zero-point fluctuations in the mode variable

$$u_{c, \text{rms}} = \sqrt{\frac{\hbar}{Xc\omega_n}}. \quad (20)$$

Now we can calculate the zero-point fluctuations of current as

$$I_n^{\text{Zpf}} = \frac{1}{Xl} \left| \frac{\partial u}{\partial x} \right|_{x=0, \text{rms}} = \sqrt{\frac{\hbar}{Xc\omega_n}} \frac{k \sin(kX)}{Xl} = \sqrt{\frac{\hbar}{Xl}} \sqrt{\frac{\omega_n}{1 + \left(\frac{\omega_n}{\omega_{\text{cutoff}}}\right)^2}}. \quad (21)$$

### Acknowledgements

This work was supported by Japan Science and Technology Agency Core Research for Evolutionary Science and Technology (Grant No. JPMJCR1775).

### Author contributions statement

Z.A., F.Y., and K.S. conceived the experiment. Z.A., F.Y., and T.F. designed the samples and performed the measurements. K.K. and S.S. fabricated the samples. S.A. performed the theoretical calculations. Z.A., S.A., F.Y., and T.F. analyzed the measurement data. Z.A. and S.A. wrote the manuscript with feedback from all authors. T.A. and K.S. supervised the project.

---

[1] Nielsen, M. A. and Chuang, I. L. *Quantum Computation and Quantum Information: 10th Anniversary Edition* (Cambridge University Press, 2010).

[2] Kimble, H. J. The quantum internet. *Nature* 453, 1023 (2008).

[3] Devoret, M. H. and Schoelkopf, R. J. Superconducting circuits for quantum information: An outlook. *Science* 339, 1169 (2013).

[4] Lamb, W. E. and Rutherford, R. C. Fine structure of the hydrogen atom by a microwave method. *Phys. Rev.* 72, 241–243 (1947).

[5] Brune, M. et al. From lamb shift to light shifts: Vacuum and subphoton cavity fields measured by atomic phase sensitive detection. *Phys. Rev. Lett.* 72, 3339–3342 (1994).

- [6] Fragner, A. et al. Resolving vacuum fluctuations in an electrical circuit by measuring the lamb shift. *Science* 322, 1357–1360 (2008).
- [7] Forn-Díaz, P., Lamata, L., Rico, E., Kono, J. and Solano, E. Ultrastrong coupling regimes of light-matter interaction. *Rev. Mod. Phys.* 91, 025005 (2019).
- [8] Frisk Kockum, A., Miranowicz, A., De Liberato, S., Savasta, S. and Nori, F. Ultrastrong coupling between light and matter. *Nat. Rev. Phys.* 1, 025005 (2019).
- [9] Yoshihara, F. et al. Superconducting qubit–oscillator circuit beyond the ultrastrong-coupling regime. *Nat. Phys.* 13, 44 (2017).
- [10] Yoshihara, F. et al. Characteristic spectra of circuit quantum electrodynamics systems from the ultrastrong- to the deep-strong-coupling regime. *Phys. Rev. A* 95, 053824 (2017).
- [11] Anappara, A. A. et al. Signatures of the ultrastrong light-matter coupling regime. *Phys. Rev. B* 79, 201303 (2009).
- [12] Gambino, S. et al. Exploring light–matter interaction phenomena under ultrastrong coupling regime. *ACS Photonics* 1, 1042 (2014).
- [13] Benz, F. et al. Single-molecule optomechanics in “picocavities”. *Science* 354, 726–729 (2016).
- [14] Bayer, A. et al. Terahertz light–matter interaction beyond unity coupling strength. *Nano Lett.* 17, 6340 (2017).
- [15] Blais, A., Huang, R.-S., Wallraff, A., Girvin, S. M. and Schoelkopf, R. J. Cavity quantum electrodynamics for superconducting electrical circuits: An architecture for quantum computation. *Phys. Rev. A* 69, 062320 (2004).
- [16] Wallraff, A. et al. Strong coupling of a single photon to a superconducting qubit using circuit quantum electrodynamics. *Nature* 431, 162–167 (2004).
- [17] Chiorescu, I. et al. Coherent dynamics of a flux qubit coupled to a harmonic oscillator. *Nature* 431, 159 (2004).
- [18] Bourassa, J. et al. Ultrastrong coupling regime of cavity qed with phase-biased flux qubits. *Phys. Rev. A* 80, 032109 (2009).
- [19] Niemczyk, T. et al. Circuit quantum electrodynamics in the ultrastrong-coupling regime. *Nat. Phys.* 6, 772–776 (2010).
- [20] Lizuain, I., Casanova, J., García-Ripoll, J. J., Muga, J. G. and Solano, E. Zeno physics in ultrastrong-coupling circuit qed. *Phys. Rev. A* 81, 062131 (2010).
- [21] Forn-Díaz, P. et al. Observation of the bloch-siegert shift in a qubit-oscillator system in the

ultrastrong coupling regime. *Phys. Rev. Lett.* 105, 237001 (2010).

[22] Felicetti, S., Romero, G., Rossini, D., Fazio, R. and Solano, E. Photon transfer in ultrastrongly coupled three-cavity arrays. *Phys. Rev. A* 89, 013853 (2014).

[23] Forn-Díaz, P. et al. Ultrastrong coupling of a single artificial atom to an electromagnetic continuum in the nonperturbative regime. *Nat. Phys.* 13, 39 (2017).

[24] Sundaresan, N. M. et al. Beyond strong coupling in a multimode cavity. *Phys. Rev. X* 5, 021035 (2015).

[25] Liu, Y. and Houck, A. A. Quantum electrodynamics near a photonic bandgap. *Nat. Phys.* 13, 48 (2017).

[26] Bosman, S. J. et al. Multi-mode ultra-strong coupling in circuit quantum electrodynamics. *npj Quantum Inf.* 3, 46 (2017).

[27] Martínez, J. P. et al. A tunable josephson platform to explore many-body quantum optics in circuit-qed. *npj Quantum Inf.* 5, 19 (2019).

[28] Koshino, K., Shitara, T., Ao, Z. and Semba, K. Deterministic three-photon down-conversion by a passive ultrastrong cavity-qed system. *Phys. Rev. Res.* 4, 013013 (2022).

[29] Yoshihara, F. et al. Inversion of qubit energy levels in qubit-oscillator circuits in the deep-strong-coupling regime. *Phys. Rev. Lett.* 120, 183601 (2018).

[30] Yoshihara, F., Ashhab, S., Fuse, T., Bamba, M. and Semba, K. Hamiltonian of a flux qubit-lc oscillator circuit in the deep-strong-coupling regime. *Sci. Rep.* 12, 6764 (2022).

[31] Gely, M. F. et al. Convergence of the multimode quantum rabi model of circuit quantum electrodynamics. *Phys. Rev. B* 95, 245115 (2017).

[32] Malekakhlagh, M., Petrescu, A. and Türeci, H. E. Cutoff-free circuit quantum electrodynamics. *Phys. Rev. Lett.* 119, 073601 (2017).

[33] Ashhab, S. and Nori, F. Qubit-oscillator systems in the ultrastrong-coupling regime and their potential for preparing nonclassical states. *Phys. Rev. A* 81, 042311 (2010).